Acta Crystallographica Section D
Biological Crystallography
ISSN 0907-4449

Conformational switches in winged-helix domains 1 and 2 of bacterial translation elongation factor SelB

Oleg Ganichkin and Markus C. Wahl*

Max-Planck-Institut für Biophysikalische Chemie, Makromolekulare Röntgenkristallographie, Am Fassberg 11, D-37077 Göttingen, Germany

Correspondence e-mail: mwahl@gwdg.de

Received 9 July 2007
Accepted 28 August 2007

PDB Reference: WH1 and WH2 motifs of SelB, 2v9v, r2v9vsf.

The crystal structure of the first two winged-helix motifs of translation elongation factor SelB from *Moorella thermoacetica* has been determined at 1.1 Å resolution. Compared with the previous structure of the two domains in conjunction with winged-helix modules 3 and 4, the first winged-helix domain underwent a substantial conformational change during which the α-helical and β-sheet portions of the element opened up like a shell. This conformational rearrangement was elicited by a change in the orientation of Trp396, leading to the disclosure of a bona fide ligand-binding site in the direct vicinity of Trp396. Additionally, the C-terminal tail of the second domain followed a different path compared with the previous structure. It is conceivable that these conformational switches constitute part of the molecular mechanism that underlies the communication between the N-terminal part of SelB, which binds Sec-tRNA^{Sec} and GTP, and the C-terminal part of the protein, which binds selenocysteine-insertion sequences.

1. Introduction

In all three lines of descent, multi-factorial machineries have evolved to sustain the co-translational incorporation of a 21st amino acid, selenocysteine (Sec), into proteins (reviewed in Stadtman, 1996; Cobucci-Ponzano *et al.*, 2005; Allmang & Krol, 2006; Hatfield *et al.*, 2006). Invariably, Sec is incorporated in response to a reprogrammed UGA codon (Zinoni *et al.*, 1987; Berry, Banu & Larsen, 1991; Wilting *et al.*, 1997). In the framework of a conventional mRNA, UGA functions as a translational stop signal. Reprogramming of UGA into a Sec codon is achieved by means of a selenocysteine-insertion sequence (SECIS) on the selenoprotein mRNA. In bacterial selenoprotein mRNAs, SECIS elements are irregular stem-loop structures directly downstream of the UGA codon and within the open reading frames (Zinoni *et al.*, 1990). In archaea (Wilting *et al.*, 1998; Rother *et al.*, 2001) and eukaryotes (Berry, Banu, Chen *et al.*, 1991; Berry *et al.*, 1993), SECIS elements occur in the 3′-untranslated region or, in one case (Wilting *et al.*, 1998), the 5′-untranslated region.

The bacterial SECIS elements are recognized by elongation factor SelB (Baron *et al.*, 1993; Ringquist *et al.*, 1994), a multifunctional protein. The N-terminal domains I–III of the protein exhibit homology to EF-Tu (Forchhammer *et al.*, 1989; Kromayer *et al.*, 1996). This part of SelB binds GTP and in

addition specifically and exclusively recognizes the specialized tRNA^{Sec} after it has been charged with Sec (Kromayer *et al.*, 1996; Leibundgut *et al.*, 2005). tRNA^{Sec} exhibits a UCA anticodon to read the Sec-UGA codon (Leinfelder *et al.*, 1988). The C-terminal domain IV of bacterial SelB has no homologous part in EF-Tu. It binds the SECIS element (Kromayer *et al.*, 1996) and thereby increases the concentration of Sec-tRNA^{Sec} on the selenoprotein mRNA in close proximity to the Sec-UGA codon. The factor ensemble required for the recognition of SECIS elements and (Sec)-tRNA^{Sec} is more complex in archaea and eukaryotes than in bacteria (recently reviewed in Cobucci-Ponzano *et al.*, 2005; Allmang & Krol, 2006; Hatfield *et al.*, 2006).

The functionally defined domain IV of bacterial SelB structurally comprises an array of four winged-helix (WH) units (Selmer & Su, 2002). The domain pairs WH1/2 and WH3/4 are each linearly arrayed and the two pairs of domains adopt an overall 'L' shape (Selmer & Su, 2002; Fig. 1). Domains WH3/4 are sufficient for high-affinity binding to a SECIS element (Kromayer *et al.*, 1996; Yoshizawa *et al.*, 2005). The structure of *Moorella thermoacetica* (*mth*) SelB WH3/4 in complex with a SECIS element has recently revealed the molecular basis of RNA recognition by WH domains (Yoshizawa *et al.*, 2005). Whether the first two WH domains embody a particular function apart from constituting a spacer between the terminal business ends of SelB is presently unclear.

A number of findings have suggested that the N-terminal EF-Tu-like domains and the SECIS-binding WH3/4 domains functionally interact with each other. For instance, binding of Sec-tRNA^{Sec} to SelB increases the affinity of the factor for a SECIS element (Baron *et al.*, 1993; Thanbichler *et al.*, 2000). Furthermore, interaction with a SECIS element promotes the GTPase activity of SelB (Hüttenhofer & Böck, 1998). Since the structure of the quarternary SelB–GTP–Sec-tRNA^{Sec}–SECIS complex is presently not available, the molecular mechanism underlying this functional communication is unclear. Little structural change was observed within the SECIS-binding WH3/4 domains upon interaction with the mRNA (Yoshizawa *et al.*, 2005), suggesting that domains WH3/4 may not directly communicate SECIS binding to the N-terminal portion of SelB. It has been suggested that the WH3/4 domains are flexibly hinged to the

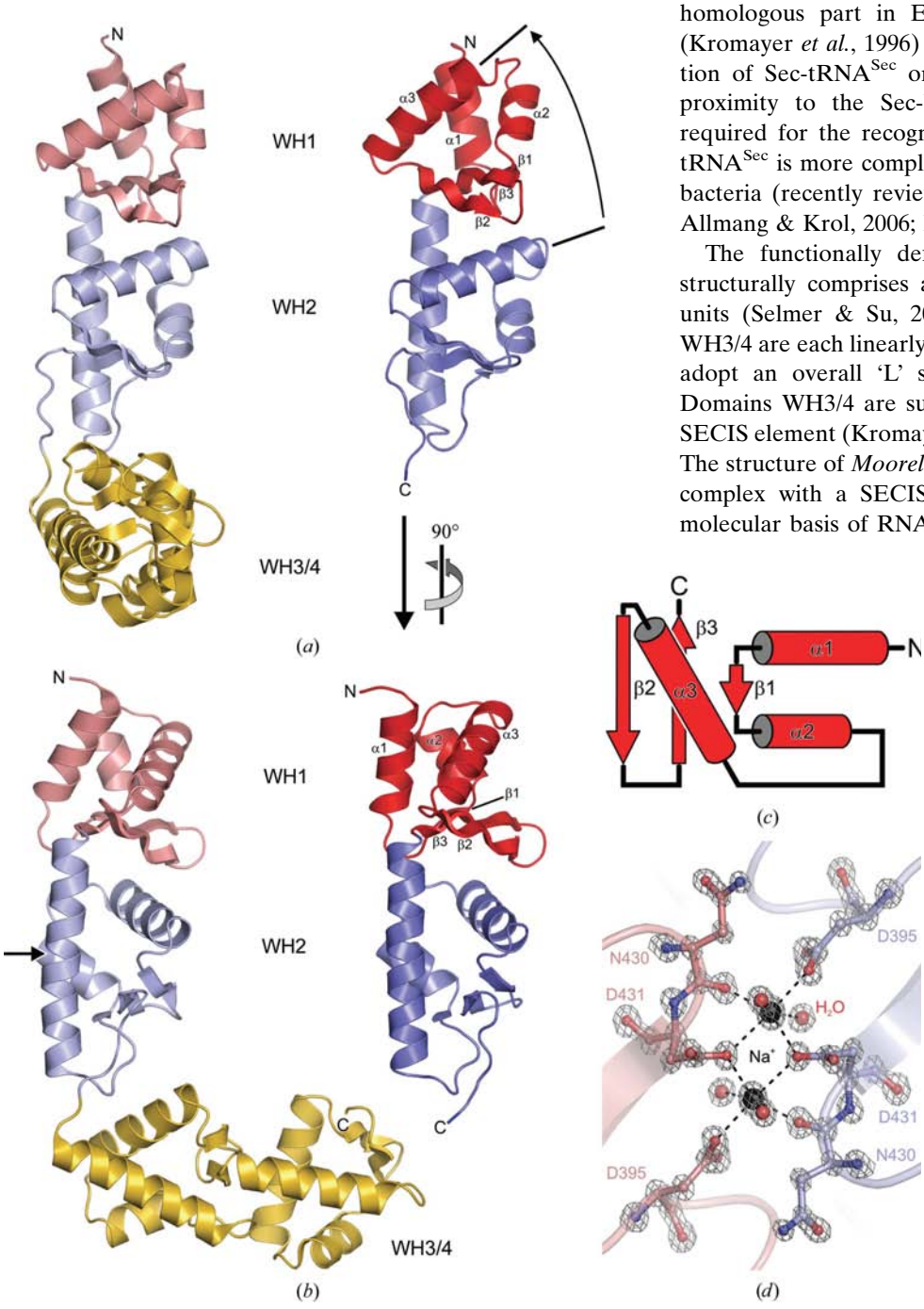

Figure 1
(*a*) and (*b*) Comparison of the previously determined WH1–4 structure of *mth*SelB (left; PDB code 1lva; Selmer & Su, 2002) with the present structure of domains WH1/2 (right). WH1, WH2 and WH3/4 of the WH1–4 structure are shown in light red, light blue and gold, respectively. WH1 and WH2 of the present structure are shown in red and blue, respectively. Secondary-structure elements of WH1 of the present structure are labelled. N, N-terminus; C, C-terminus. The view in (*b*) is orthogonal to that in (*a*), as indicated. The arrow in (*a*) emphasizes the change in the angle between the helical axes of the two neighbouring α3 helices, representative of the conformational switch in WH1. An arrow in (*b*) indicates a bend of $\sim$7° in helix α1 of WH2 that is not seen in the present structure, in which the helix is straight. (*c*) Schematic representation of the topology of the WH domains. (*d*) $2F_o - F_c$ electron density (grey mesh) contoured at the 3σ level in the region of a crystal-packing motif involving two sodium ions (black spheres), water molecules (red spheres) and protein residues 395, 430 and 431 (ball-and-stick representation; C atoms are colour-coded according to the respective protein; nitrogen, blue; oxygen, red).

WH1/2 domains (Selmer & Su, 2002), which in turn may be flexibly connected to the EF-Tu homology portion. Communication between the peripheral portions could take place *via* these flexible connections (Selmer & Su, 2002). However, the functional coupling of the terminal portions of SelB also draws the attention to the WH1/2 domains themselves, which constitute the connector between the Sec-tRNA^{Sec}/GTP-binding portion and the SECIS-binding portion of SelB. Here, we address these questions by a comparative structural analysis of the first two WH domains of *mth*SelB.

2. Materials and methods

2.1. Cloning, expression and purification

A DNA fragment encoding the WH1 and WH2 motifs of *mth*SelB (amino acids 377–511) was amplified from *M. thermoacetica* genomic DNA by PCR and cloned into plasmid pETM-11 (http://www.embl.de/ExternalInfo/protein_unit/draft_frames/frame_which_vector_ext.htm) to allow the expression of an N-terminally His_6-tagged protein. The insert was verified by DNA sequencing. Rosetta2(DE3) cells were transformed with the *mth*SelB$^{377–511}$ expression construct. Overproduction of the target protein was carried out at 289 K using auto-inducing medium (Studier, 2005). Cells were harvested when the maximum culture density was reached and resuspended in buffer *A* (10 m*M* HEPES–NaOH pH 7.5, 200 m*M* NaCl). After cell rupture by sonication and removal of cell debris by centrifugation, the soluble fusion protein was captured on an Ni–NTA Sepharose column, washed with buffer *B* (10 m*M* HEPES–NaOH pH 7.5, 1 *M* NaCl, 20 m*M* imidazole) and eluted with buffer *C* (10 m*M* HEPES–NaOH pH 7.5, 200 m*M* NaCl, 250 m*M* imidazole). TEV protease was added to the eluate and the mixture was dialyzed against buffer *A* overnight. The sample was again passed over Ni–NTA Sepharose, collecting *mth*SelB$^{377–511}$ without a tag in the flowthrough.

2.2. Crystallographic analysis

For crystallization, 1 µl *mth*SelB$^{377–511}$ at 8.5 mg ml^{-1} was mixed with 1 µl reservoir solution (100 m*M* HEPES–NaOH pH 6.9–7.9, 3.9–4.5 *M* NaCl). Crystals were grown by hanging-drop vapour diffusion at 293 K. They were directly frozen in a 100 K cryogenic nitrogen stream. Diffraction data were collected from a cryocooled crystal at beamline PXII of the Swiss Light Source (Villigen, Switzerland) and processed using the *HKL* package (Otwinowski & Minor, 1997). The structure was solved by molecular replacement with *MOLREP* (Vagin & Teplyakov, 2000) using the coordinates for residues 377–511 of PDB entry 1lva (Selmer & Su, 2002) as a search model. Refinement proceeded by alternate cycles of model building and restrained positional/temperature-factor optimization with *REFMAC*5 (Murshudov *et al.*, 1997). All residues (377–511) could be unequivocally located in the electron density. Water molecules were automatically added with *ARP*/*wARP* (Perrakis *et al.*, 1999) and the water structure was checked and completed manually. Four chloride ions and two sodium ions (Fig. 1*d*) were located based on the coordination spheres and positive difference densities after placement of water molecules at these positions. 14 amino-acid residues were refined with two alternative conformations. In the final refinement cycles, H atoms were automatically placed on the protein structure with *REFMAC*5 and temperature factors were refined anisotropically for all heavier atoms and ions. Refinement converged at acceptable crystallographic *R* factors and geometry (Table 1).

Table 1
Crystallographic data and refinement.

Values in parentheses are for the highest resolution shell.

Data collection	
Wavelength (Å)	0.80
Temperature (K)	100
Space group	*C*2
Unit-cell parameters (Å, °)	a = 65.33, b = 46.01, c = 58.66, β = 120.43
Resolution (Å)	20.0–1.1 (1.2–1.1)
Unique reflections	61009 (13455)
Completeness (%)	100.0 (100.0)
Redundancy	7.0 (6.9)
$I/\sigma(I)$	10.0 (3.4)
$R_{sym}(I)$† (%)	8.7 (24.5)
Refinement	
Resolution (Å)	20.0–1.1 (1.128–1.1)
No. of reflections	57911 (3094)
Completeness (%)	100.0 (99.9)
Reflections in test set (%)	5.1
R_{work}‡ (%)	12.0 (15.5)
R_{free}‡ (%)	14.1 (18.2)
ESU§ (Å)	0.015
Refined atoms	
Protein molecules/residues/atoms/protons	1/135/2387/1179
Water O atoms	358
Na^+/Cl^- ions	2/4
Mean *B* factors (Å^2)	
Wilson	6.5
Protein	8.4
Water	22.4
Na^+/Cl^- ions	12.7
Ramachandran plot¶ (%)	
Favoured	99.0
Allowed	1.0
Outliers	0
R.m.s.d. from target geometry	
Bond lengths (Å)	0.014
Bond angles (°)	1.55
R.m.s.d. isotropic thermal factors (Å^2)	
Main-chain bonds	1.40
Main-chain angles	2.07
Side-chain bonds	2.96
Side-chain angles	4.15
PDB code	2v9v

† $R_{sym}(I) = \sum_{hkl}\sum_i |I_i(hkl) - \langle I(hkl)\rangle|/\sum_{hkl}\sum_i |I_i(hkl)|$ for n independent reflections and i observations of a given reflection; $\langle I(hkl)\rangle$ is the average intensity of the i observations. ‡ $R = \sum_{hkl} ||F_{obs}| - |F_{calc}||/\sum_{hkl} |F_{obs}|$; R_{work} is for reflections that do not belong to the test set and R_{free} is for reflections that belong to the test set. § ESU, estimated overall coordinate error based on maximum likelihood. ¶ Calculated with *MolProbity* (http://molprobity.biochem.duke.edu/; Davis *et al.*, 2004).

3. Results

3.1. Overall fold

We have determined an atomic resolution crystal structure of residues 377–511 of *mth*SelB (*mth*SelB$^{377–511}$) encom-

passing the first two WH domains (Table 1, Fig. 1). Globally, the two modules resemble the structure of the domains in the framework of the entire C-terminal portion of the protein (residues 377–634; Selmer & Su, 2002; Figs. 1*a* and 1*b*). Each domain is composed of three α-helices and a three-stranded antiparallel β-sheet (Fig. 1*c*). The three α-helices form a short bundle that stands like a tripod on the β-sheet (Fig. 1*a*). The β-sheet of the first domain rests on the helical bundle of the second domain, giving rise to alternating levels of α-helices and β-strands along the structure (Figs. 1*a* and 1*b*).

3.2. Global conformational changes

Although the sequences of the proteins are identical, superimposition of the present structure and the corresponding portion of the WH1–4 structure (Selmer & Su, 2002) yields a root-mean-square deviation (r.m.s.d.) of 1.75 Å for the 135 common C^{α} atoms (Figs. 1*a* and 1*b*), indicating a significant conformational difference. When the two structures are aligned with respect to the WH2 domains, the upper portions of the WH1 domains adopt different relative orientations. In part, the positional change in WH1 is the consequence of a bend of $\sim$7° in the centre helix α1 of WH2 in the WH1–4 structure (marked with an arrow in Fig. 1*b*); the same element of the present structure is straight. More importantly, the helical bundles in the two WH1 domains adopt different positions with respect to the WH1 β-sheets (Figs. 1 and 2). The entire three-helix bundle of WH1 moves like a rigid entity, since the α-helical subdomains of the two WH1 modules alone superimpose closely (r.m.s.d. of 0.81 Å for 44 common C^{α} positions). In the present structure, the three-helix bundle of WH1 has separated from the β-sheet at the side of helix α3, the apparent movement resembling the opening of a lid (Fig. 1*a*).

3.3. Local conformational switch in WH1

The global conformational rearrangement can be traced to a local reorganization of a particular residue. At the interface region of helix α3 and the β-sheet of WH1, the side chain of

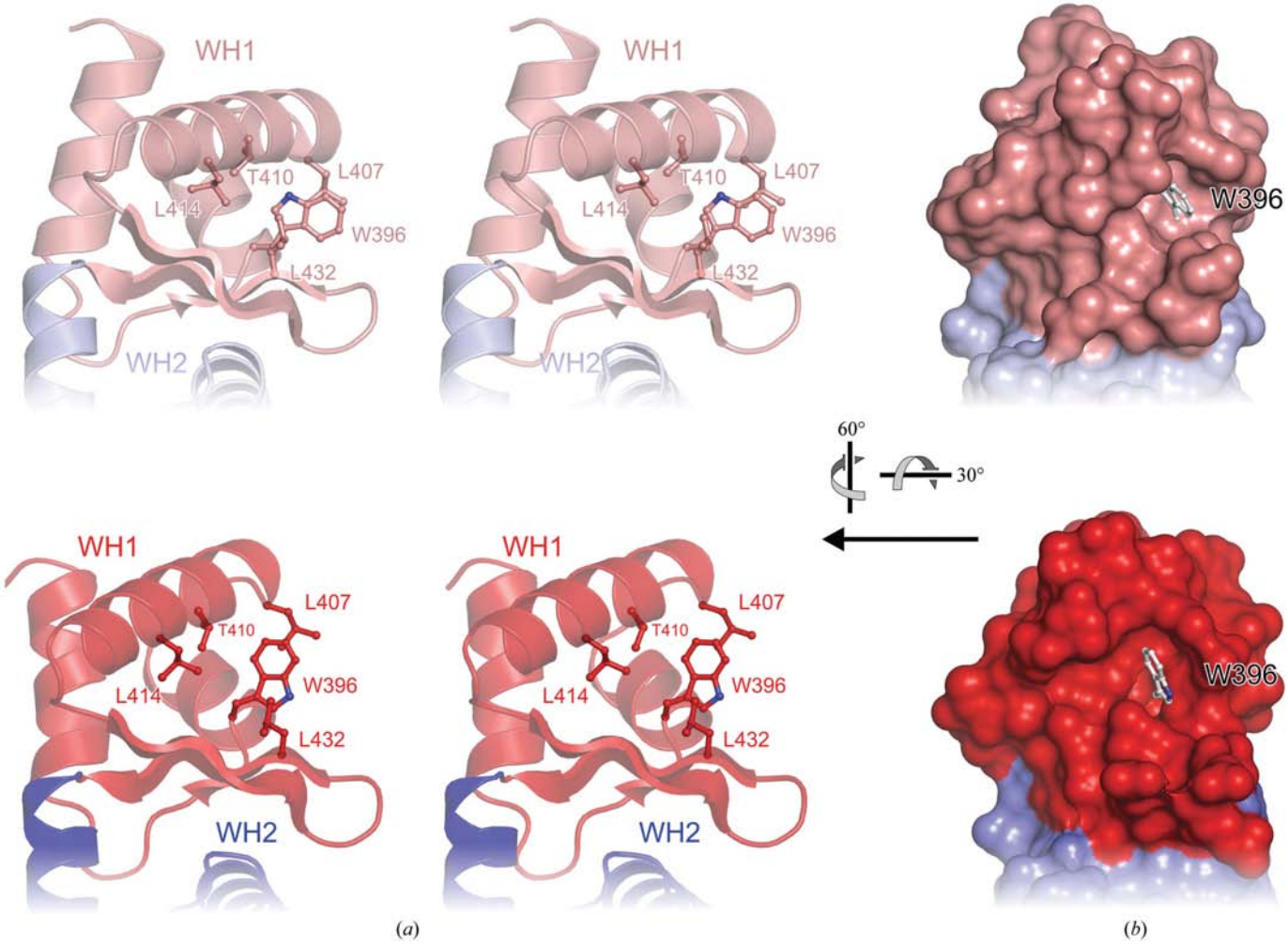

Figure 2
(*a*) Stereo ribbon plots comparing WH1 of the previous WH1–4 structure (top) and the present structure (bottom). The colouring of the domains is the same as in Fig. 1. Trp396 and neighbouring residues are shown in ball-and-stick representation and are colour-coded as before. (*b*) Surface views of the same regions of the two crystal structures with Trp396 shown in ball-and-stick representation (carbon, grey). The Trp396 pocket adapts upon rearrangement of the Trp396 side chain. The view in (*b*) is the same as in Fig. 1(*a*). In (*a*) the structures are rotated 30° about the horizontal axis and 60° about the vertical axis, as indicated.

Trp396 adopts a different orientation compared with that in the previous structure (Fig. 2*a*). The $C^{\beta}-C^{\gamma}$ dihedral angle of Trp396 has changed by almost 180°. As a consequence, the five-membered portion of the indole ring of Trp396 is proximal to helix α3 in the previous structure, while the bulkier six-membered part of the indole ring is rotated towards helix α3 in the present structure (Fig. 2*a*). Thus, in our structure the bulk of Trp396 is wedged between helix α3 and the β-sheet. Despite the different orientation of the Trp396 side chain, it remains tightly packed in a hydrophobic pocket formed by Leu407, Thr410, Leu414 (all originating from α3) and Leu432 (originating from β3; Fig. 2*a*). The latter four residues adjust slightly and together with the overall movement of the helices reshape the pocket for Trp396 (Fig. 2*a*).

3.4. Emergence of a bona fide ligand-binding site

Surface rendering of the molecules reveals that a short channel is opened up in the present structure directly neighbouring Trp396 and on the underside of helix α3 (Fig. 2*b*). In the previous WH1–4 structure (Selmer & Su, 2002) this channel is completely occluded by the backbone of helix α3 and the side chains originating from this element (Fig. 2*b*). The dimensions of the uncovered cleft appear to be suitable for the binding of a ligand, such as a short stretch of protein or nucleic acid. Indeed, the C-terminal tail of a neighbouring molecule in the crystal lattice is inserted snugly into this cleft (Fig. 3*a*). The C-terminal Phe511 side chain of this neighbour is placed perpendicularly to the indole ring of Trp 396 and may push it under helix α3 (Fig. 3*a*).

Interestingly, the location of the neighbouring peptide and in particular of Phe511 resembles the position of a guanine nucleotide from a SECIS element on the WH4 module in a previously determined SelB WH3/4–SECIS cocrystal structure (Fig. 3*b*; Yoshizawa *et al.*, 2005). While the present paper was in preparation, two additional structures of C-terminal portions of SelB in complex with SECIS elements were reported (Soler *et al.*, 2007; Ose *et al.*, 2007). In these structures, nucleotides bulged out from the stem or the apical loop of the SECIS elements again interact at the equivalent binding sites on the WH3 and WH4 elements of SelB, respectively.

Thus, although the conformational change we observe in the WH1 domain correlates with a crystal lattice contact and we presently cannot attribute cause and effect, the contact site for a neighbouring molecule that emerges in our crystal structure resembles an authentic ligand-binding site in homologous domains. Together, these observations suggest that the WH domains of SelB harbour prominent ligand-binding sites underneath helix α3 which may bind RNA or protein molecules.

3.5. Flexibility of the connecting peptide between WH2 and WH3

The two pairs of WH domains in the *mth*SelB WH1–4 structure (Selmer & Su, 2002) adopt an L shape. This orientation of the WH-domain pairs is apparently stabilized by a salt bridge between Arg461 of WH2 and Glu552 of WH3 (Selmer & Su, 2002). Co-variation of the two interacting residues suggests that this salt bridge is conserved throughout bacterial SelB molecules (Selmer & Su, 2002). In *Escherichia coli* (*eco*) SelB, a mutation that destroys this salt bridge relaxed the stringency of the SECIS recognition (Kromayer *et al.*, 1999). Based on these findings and molecular modelling, which demanded a more elongated structure of SelB on the ribosome than that observed in the crystal, Selmer and Su suggested that SECIS binding leads to a functionally important conformational change in the factor (Selmer & Su, 2002).

In the present structure, the lack of WH3 occludes the possibility of a WH2–WH3 salt bridge. Under these conditions, the C-terminal tail of domain WH2 starting at residue 504, directly after the third strand of the WH2 β-sheet, follows

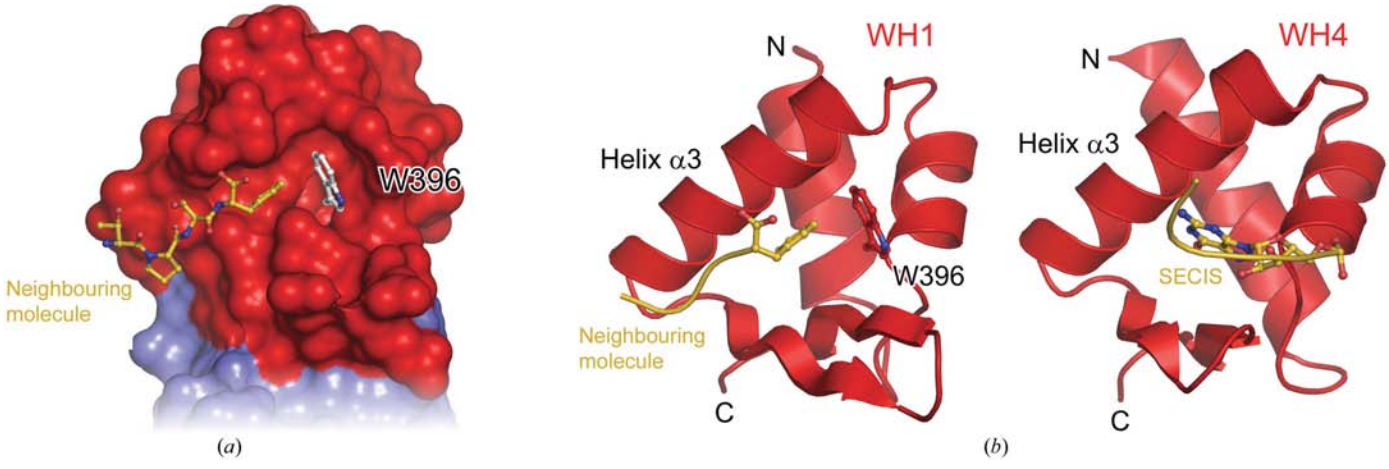

Figure 3
(*a*) Interaction of the WH1 domain of the present crystal structure (red surface; Trp396 in ball-and-stick representation; carbon, grey) with the C-terminal tail of a neighbouring molecule (ball-and-stick representation; carbon, gold). (*b*) Comparison of the interaction mode of WH1 in the present structure with the C-terminal tail of a neighbouring molecule (left) and the interaction mode of WH4 of *mth*SelB with a SECIS element (right; Ose *et al.*, 2007). WH domains are shown as red ribbon plots. Trp396 of WH1 is shown in ball-and-stick representation (carbon, red). Ligands are shown as a combination of ribbon and ball-and-stick representations (carbon and phosphorus, gold). Helices α3 and the N- and C-termini of the WH modules are labelled. Views are the same as in Fig. 2(*b*).

a different path compared with the WH2–WH3 linker peptide of the WH1–4 structure (Figs. 1*a* and 1*b*). Instead, the present WH2 terminus closely resembles the WH2–WH3 linker in a structure of *mth*SelB WH1–4 in complex with a SECIS element (Ose *et al.*, 2007). In this latter structure, the salt bridge connecting WH2 and WH3 is broken, yet the domains remain in a fixed relative orientation owing to crystal-packing interactions *via* a neighbouring SECIS element. The path of the WH2 C-terminal tails in the above structures appears to be additionally governed by a hydrogen bond from the Leu504 backbone NH to the side chain of His455 from the first helix of WH2 and by stacking of the side chains of His455 and Phe507. The different pH values under which the present crystals (pH 6.9–7.9), those of the *mth*SelB WH1–4 structure (pH 6.2) and those of the *mth*SelB WH1–4 in complex with a SECIS element (pH 5.5) were obtained may have influenced these ionic interactions.

Together, these observations corroborate the previous notion that the connection between the two pairs of WH domains, WH1/2 and WH3/4, is flexible and allows different relative orientations of the domain pairs after disruption of the Arg461–Glu552 salt bridge (Selmer & Su, 2002). In further agreement with this suggestion, the recent crystal structure of *eco*SelB WH3/4 in complex with a SECIS element showed that SECIS binding sequestered Arg524 (the equivalent of Glu552 in the reciprocal WH2–WH3 salt bridge in *eco*SelB) in the formation of a SECIS-binding pocket (Soler *et al.*, 2007). By sequestration of Arg524, SECIS binding could lead to breakage of the WH2–WH3 salt bridge, giving rise to increased flexibility as required during the subsequent interaction of SelB with the ribosome.

4. Discussion

The EF-Tu-like portion and the SECIS-binding WH3/4 part of bacterial SelB have to adopt defined relative orientations on the ribosome in order to allow concomitant interaction with Sec-tRNA^{Sec}, which approaches the ribosomal A-site where the Sec-UGA codon appears, and the SECIS element at the mRNA entrance channel. A defined but different orientation may also exist off the ribosome, explaining the cooperative binding of Sec-tRNA^{Sec} and the SECIS element to SelB. Most likely, the domain arrangement changes upon release of Sec-tRNA^{Sec} into the ribosomal A-site (Selmer & Su, 2002), which could lead to the somewhat reduced affinity of SelB for the SECIS element (Thanbichler *et al.*, 2000) and which could thereby facilitate the detachment of the factor from the mRNA. Otherwise, SelB would represent a roadblock for the progressing ribosome. No significant structural changes were seen in WH3/4 upon SECIS binding (Yoshizawa *et al.*, 2005). Instead, our results attest to the capacity of WH1/2 to undergo conformational changes. These conformational changes may be instrumental for functional communication between the N-terminal EF-Tu-like domains and the C-terminal SECIS-binding domains of SelB.

The different orientation of the C-terminal tail of WH2 (residues 504–511) in the present structure compared with the *mth*SelB WH1–4 structure directly supports the notion of a global repositioning of the two pairs of WH modules upon interaction of SelB with the ribosome. While different crystallization pH values may have contributed to the different orientations observed in the various crystal structures, it is conceivable that similar rearrangements are elicited by changing molecular interactions *in vivo*. The relative movement of the domains would be enabled by conformational flexibility about the WH2–WH3 linker coupled to breakage of a conserved salt bridge connecting the two WH modules (Selmer & Su, 2002). The latter notion has been independently supported by recent crystal structures of *mth*SelB WH1–4 in complex with SECIS elements (Soler *et al.*, 2007; Ose *et al.*, 2007). Interestingly, the WH1 domain was not visible in these latter crystal structures. The dynamic disorder of WH1 in these structures suggests that the link between the first two WH modules is also flexible. Therefore, rearrangement of the relative orientations of domains WH1 and WH2 may contribute to the conformational adjustments of SelB in different functional states.

The conformational switch observed here within WH1 could also have long-range effects on the structure of SelB. When the previous WH1–4 structure is superimposed on WH1 helices α1–3 or, alternatively, on WH2 of the present structure, the tip of the WH4 domain changes position by $\sim$20 Å. It has been calculated that a conformational change in SelB WH1–4 that allows it to traverse an additional distance of 15–25 Å may be required on the ribosome in order to bridge between the ribosomal A-site (where the Sec-UGA codon appears) and the mRNA entrance channel (where the SECIS element is positioned; Selmer & Su, 2002). Possibly, part of this distance can be covered by a conformational response in WH1 as observed here.

Domains I–III of SelB and portions of the 16S rRNA are candidate ligands that could interact at the putative ligand-binding site disclosed by the conformational change in WH1 in the present structure. For example, it has been suggested that the WH1/2 region of SelB may interact with helix 16 or helix 33 of the 16S rRNA upon SelB binding to the ribosome (Yoshizawa *et al.*, 2005). In addition, a direct contact of domains I–III of SelB to WH1 has been discussed (Soler *et al.*, 2007). In summary, the data presented here suggest that the WH1/2 element may serve as a malleable link rather than as a rigid spacer between the two business ends of bacterial SelB, thereby allowing them to adopt various functional orientations.

This work was supported by a grant from the Deutsche Forschungsgemeinschaft (WA1126/2-3) and the Max-Planck-Society. We thank the staff of beamline PXII of the Swiss Light Source (Villigen, Switzerland) for excellent support during data collection.

References

Allmang, C. & Krol, A. (2006). *Biochimie*, **88**, 1561–1571.

Baron, C., Heider, J. & Böck, A. (1993). *Proc. Natl Acad. Sci. USA*, **90**, 4181–4185.
Berry, M. J., Banu, L., Chen, Y. Y., Mandel, S. J., Kieffer, J. D., Harney, J. W. & Larsen, P. R. (1991). *Nature (London)*, **353**, 273–276.
Berry, M. J., Banu, L., Harney, J. W. & Larsen, P. R. (1993). *EMBO J.* **12**, 3315–3322.
Berry, M. J., Banu, L. & Larsen, P. R. (1991). *Nature (London)*, **349**, 438–440.
Cobucci-Ponzano, B., Rossi, M. & Moracci, M. (2005). *Mol. Microbiol.* **55**, 339–348.
Davis, I. W., Murray, L. W., Richardson, J. S. & Richardson, D. C. (2004). *Nucleic Acids Res.* **32**, W615–W619.
Forchhammer, K., Leinfelder, W. & Böck, A. (1989). *Nature (London)*, **342**, 453–456.
Hatfield, D. L., Carlson, B. A., Xu, X. M., Mix, H. & Gladyshev, V. N. (2006). *Prog. Nucleic Acid Res. Mol. Biol.* **81**, 97–142.
Hüttenhofer, A. & Böck, A. (1998). *Biochemistry*, **37**, 885–890.
Kromayer, M., Neuhierl, B., Friebel, A. & Böck, A. (1999). *Mol. Gen. Genet.* **262**, 800–806.
Kromayer, M., Wilting, R., Tormay, P. & Böck, A. (1996). *J. Mol. Biol.* **262**, 413–420.
Leibundgut, M., Frick, C., Thanbichler, M., Böck, A. & Ban, N. (2005). *EMBO J.* **24**, 11–22.
Leinfelder, W., Zehelein, E., Mandrand-Berthelot, M. A. & Böck, A. (1988). *Nature (London)*, **331**, 723–725.
Murshudov, G. N., Vagin, A. A. & Dodson, E. J. (1997). *Acta Cryst.* D**53**, 240–255.
Ose, T., Soler, N., Rasubala, L., Kuroki, K., Kohda, D., Fourmy, D., Yoshizawa, S. & Maenaka, K. (2007). *Structure*, **15**, 577–586.
Otwinowski, Z. & Minor, W. (1997). *Methods Enzymol.* **276**, 307–326.
Perrakis, A., Morris, R. & Lamzin, V. S. (1999). *Nature Struct. Biol.* **6**, 458–463.
Ringquist, S., Schneider, D., Gibson, T., Baron, C., Böck, A. & Gold, L. (1994). *Genes Dev.* **8**, 376–385.
Rother, M., Resch, A., Gardner, W. L., Whitman, W. B. & Böck, A. (2001). *Mol. Microbiol.* **40**, 900–908.
Selmer, M. & Su, X.-D. (2002). *EMBO J.* **21**, 4145–4153.
Soler, N., Fourmy, D. & Yoshizawa, S. (2007). *J. Mol. Biol.* **370**, 728–741.
Stadtman, T. C. (1996). *Annu. Rev. Biochem.* **65**, 83–100.
Studier, F. W. (2005). *Protein Expr. Purif.* **41**, 207–234.
Thanbichler, M., Böck, A. & Goody, R. S. (2000). *J. Biol. Chem.* **275**, 20458–20466.
Vagin, A. & Teplyakov, A. (2000). *Acta Cryst.* D**56**, 1622–1624.
Wilting, R., Schorling, S., Persson, B. C. & Böck, A. (1997). *J. Mol. Biol.* **266**, 637–641.
Wilting, R., Vamvakidou, K. & Böck, A. (1998). *Arch. Microbiol.* **169**, 71–75.
Yoshizawa, S., Rasubala, L., Ose, T., Kohda, D., Fourmy, D. & Maenaka, K. (2005). *Nature Struct. Mol. Biol.* **12**, 198–203.
Zinoni, F., Birkmann, A., Leinfelder, W. & Böck, A. (1987). *Proc. Natl Acad. Sci. USA*, **84**, 3156–3160.
Zinoni, F., Heider, J. & Böck, A. (1990). *Proc. Natl Acad. Sci. USA*, **87**, 4660–4664.